LANGMUIR Article
Cite This: Langmuir 2019, 35, 8860−8866
pubs.acs.org/Langmuir

# Imaging the Separation Distance between the Attached Bacterial Cells and the Surface with a Total Internal Reflection Dark-Field Microscope

Aiguo Xia,[†] Shuai Yang,[†] Rongrong Zhang,[†] Lei Ni,[†] Xiaochen Xing,[*,‡] and Fan Jin[*,†,§,∥,⊥]

[†]Hefei National Laboratory for Physical Sciences at the Microscale, [‡]Department of Chemical Physics, [§]Department of Polymer Science and Engineering, and [∥]CAS Key Laboratory of Soft Matter Chemistry, University of Science and Technology of China, Hefei 230026, P. R. China

**ABSTRACT:** The attachment of bacterial cells to a surface is implicated in the formation of biofilms. Although the surface-related behaviors in this process, such as single cell motility and surface sensing, have been investigated intensively, the precise information of separation distance between the attached cells and the surface has remained unclear. Here, we set a prism-based total internal reflection dark-field microscope (p-TIRDFM) combined with the microfluidic method to image the separation distance of single attached cells. We directly observed that bacterial cells attached to the surface with one nearest touchpoint, and it gradually changed to two touchpoints, respectively, for the two offspring with the cell division. We first monitored the fluctuation of the relative distance on nanometer scale when cells twitch on a surface and further established the relationship between the twitching velocity and the separation distance. The results indicated that the moving cells are a considerable distance apart from the surface and the separation distance fluctuated more widely than immobile cells.

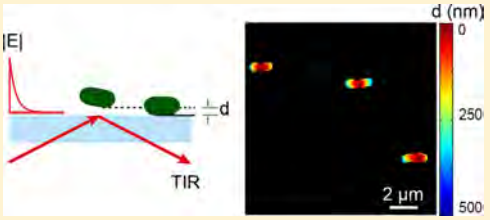


## INTRODUCTION

Total internal reflection microscopy[1] is an optical imaging technique based on the unique properties of the evanescent wave, which is generated by total internal reflection of incident light at the glass−water interface. The evanescent wave will scatter light when an object is adjacent to the glass surface, and this evanescent field decays exponentially in intensity with the distance from the interface, thereby providing a sensitive and quantitative tool to study the interactions between a colloidal particle and a glass surface through the measurement of separation distance.[2−4] With the introduction of fluorophores, an evanescent wave can selectively excite the fluorophores located in a restricted region that is in the vicinity of the glass surface, while the excitation of fluorophores in the regions farther from the surface is evaded, and this technique is called total internal reflection fluorescence microscopy (TIRFM).[5] Because the fluorescence excitation is confined within a thin zone, the signal-to-noise ratio is highly improved, where the TIRFM image usually has a low background fluorescence, virtually no out-of-focus fluorescence due to the minimal exposure of objects to light at any other planes in the sample.[5−7] When employing an objective-type evanescent illumination to produce a bright object surrounded by a dark background, researchers developed total internal reflection dark field microscopy (TIRDFM) and further obtained super-resolution dark-field images using this technique.[8−11] TIRDFM has now been widely applied in the research of biological and materials, such as single nanoparticle spectroscopy[12−14] and label-free live tissue imaging.[15−17]

In cell biology, the imaging techniques that capitalize on the properties of fluorescence could provide images with high contrast,[18−20] and the super-resolving microscopy techniques have the advantages in image resolution that reaches a sub-100 nm length scale.[19−21] However, they all have the problem that the image acquisition process needs much time or cells suffer from phototoxicity or both. In contrast, the total internal reflection-related microscopies could meet the shortcomings, where cells do not need any labeling, and the produced images have high signal-to-background ratios because of minimal exposure of cells to light. In addition, because of the unique properties of the evanescent wave, these imaging techniques cannot be used to view deeply into thick cells and have limited application in regions farther from the surface but are well suitable for the study of biochemical dynamics and surface-related behaviors of cells at cell-substrate regions. For instance, TIRFM can image the fluorescence-marked submembrane filament structure with high contrast at the substrate contact regions[22] and enable the direct observation of extension and retraction of type IV pili (TFP) of bacterial cells on the surface.[23]

Bacterial cells can quickly spread over a surface by twitching motility, and this type of bacterial movement is driven by the extension, tethering, and then retraction of TFP.[24] The twitching motility that allows bacterial cells to colonize surfaces is necessary for the formation of complex bacterial

Received: May 8, 2019
Revised: May 30, 2019
Published: June 2, 2019






DOI: 10.1021/acs.langmuir.9b01378
Langmuir 2019, 35, 8860−8866

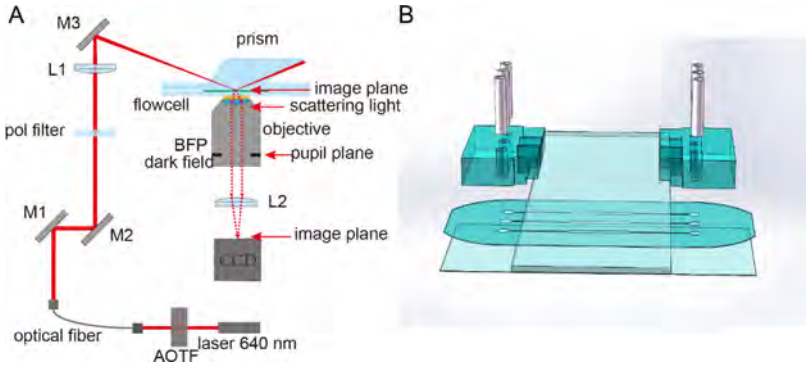


**Figure 1.** Experimental setup and the designed microfluidic device. (A) Generation of total internal reflection on a glass surface, a focused laser beam was incident perpendicularly into the prism. Bacterial cells attached on the glass slide were illuminated by the evanescent wave. The scattered light was transferred into the camera, whereas the scattered light was partially blocked in the back focal plane to enable dark-field imaging. (B) Ultrathin microfluidic device was designed with a PDMS stamp sandwiched between a glass slide and a coverslip. Total internal reflection was generated on the lower surface of the glass slide. The cover glass provided a window to image.

communities called biofilms,[25] and it is a surface-related behavior. As the model organism for study of the motility of bacterial cells, *Pseudomonas aeruginosa* has been observed twitching on the surface with TFP[24] by the high-speed camera and bright-field microscope.[26] The studies have found that there is a certain angle between attached bacterial cells and surface,[27] which indicates that the body of the attached cells is not fully in contact with the surface, but a part of the body is away from the surface. However, the more precise distance information is little known.

In nanomicrobiology, the atomic force microscope and electron microscope have facilitated the understanding of the nanoscale structural and physical properties of single bacterial cells.[28] Both of them have very high resolution but these classical techniques offer damage samples or require specific conditions. The electron microscope basically needs freezing or vacuum,[29] and the traditional atomic force microscope needs dried bacterial cells[30] or modified substrates, such as coating with gelatin, to immobilize the cells for imaging living bacterial cells.[31] Although the newly developed high-speed atomic force microscopy (HS-AFM) allows direct observation of cell and tissue dynamics in real time under physiological conditions,[32,33] this technique does not apply to the cases, where cells are cultured in a flow chamber for long-term experiments. In such particular cases, there is no operation space for the tip of HS-AFM because of the spatial constraint of the chamber, and the image acquisition per frame still needs much time for scanning compared with snapshot imaging methods. Therefore, the techniques of nano−microbiology have limited application in the imaging for long-lived bacterial cells during development in culture, including the measurement of the distance-separating cells and surface when bacterial cells are twitching on a surface. In our study, we first established a microscopy method based on a prism-based total internal reflection dark-field microscope (p-TIRDFM) to eliminate coma of total internal reflection. Subsequently, we applied this method to monitor the adhesion process of the *P. aeruginosa* cells in a designed microfluidic device, and we imaged the intensity of scattered light in the cell-glass contact regions to indicate the distance from the surface. Then, the attached cells were cultured under continuous medium in the microfluidic device, and we monitored the real-time scattering intensity of cells to characterize the change of the distance between the bacterial cells and the surface when cells are twitching on a surface. The images were analyzed on a single-cell scale. We directly observed that bacterial cells attached to the surface with one nearest touchpoint, and it gradually changed two touchpoints, respectively, for the two offspring with cell's division. We first monitored the fluctuation of the relative distance on the nanometer scale when cells are twitching on the surface and further established the relationship between the twitching velocity and the separation distance. Thus, our approach establishes a methodology for using the p-TIRDFM to study the surface-related behaviors of bacterial cells and can further promote the related modern research.

## EXPERIMENTAL SECTION

**Experimental Setup.** The schematic design of the TIRDFM is shown in Figure 1A. An acousto-optical tunable filter was equipped for rapid laser selection. The collimated polarized 640 nm laser (Andor) passed through a half-wave plate ($\lambda/2$) and then focused perpendicularly on a prism with an inclination angle of 67.8°, which results in that the evanescent wave was generated by total internal reflection at the glass−water interface. The evanescent wave can scatter light when polystyrene (PS) particles or bacterial cells used in our study are attached on the glass surface, where they are located in the evanescent field. The illuminated scattered light was collected into a sCMOS camera (Andor Neo) through a 100-fold dark field objective (Olympus 100× oil iris). Because the direction of the evanescent wave is perpendicular to the optical axis of the objective, this projects an image that is not in the center of the field to appear as wedge-shaped, known as coma. To enhance the image quality, we adjusted the numerical aperture of the dark-field objective from 1.4 to 0.6 to minimize the tail-like effects on the image.

The microfluidic device for culturing the bacterial cells contains a coverslip, a polydimethylsiloxane (PDMS) microfluidic chamber, a glass slide, an inlet part, and an outlet part (Figure 1B). A silicon substrate mold, having chambers with a height of 20 $\mu$m, width of 1.1 mm, and length of 6 mm, was first fabricated with the SU-8 2025 photoresist (microChem) process.[34] Note that the chamber is wide enough to avoid the scattered light produced by the surrounding PDMS. For preparation of the cultural device, the dimethyl siloxane monomer (SYLGARD 184) and curing agent were mixed in a 10:1 ratio. After defoaming, the mixture was poured onto the fabricated silicon wafer, and a coverslip was sunk to the bottom close to the silicon substrate. After the removal of air bubbles by vacuum, place the device (the PDMS prepolymer was sandwiched between the silicon wafer and coverslip) in an oven, set to 70 °C for a curing of 30 min. The chip containing the coverslip and the cured PDMS were cut from the silicon wafer, where the cultural channels are patterned on



DOI: 10.1021/acs.langmuir.9b01378
*Langmuir* 2019, 35, 8860−8866

the surface of PDMS opposite to the coverslip. The chip (with the patterned surface facing up) and a hydrofluoric acid-cleaned glass slide were placed in an oxygen plasma cleaner for oxidation at 50 mTorr of $H_2O$ pressures and 18 W of power for 3 min. Then, the surface patterned with channels of the chip was put on the glass slide to form a conformal contact, and the cultural device was prepared.

To make the inlet and outlet parts, a slide fixed on a flat silicon wafer serves as the master. The PDMS stamps were prepared as mentioned above and cut to fit with the cultural device. Two PDMS stamps were punched with a biopsy puncher as inlets and outlets, respectively. After the plasma treatment, two PDMS stamps containing the inlets and outlets were assembled to the cultural device, and finally, the microfluidic device was fabricated (Figure 1B). The device was placed at 80 °C overnight for further curing.

In our microfluidic device (Figure 1B), an ultra-thin PDMS stamp was sandwiched between a glass slide and a coverslip. The chamber is located between the glass slide and the patterned surface of the PDMS stamp, where the total internal reflection was generated on the lower surface of the glass slide. The cover glass slide provided a window to image the attached cells on the lower surface of the glass slide, and the ultrathin PDMS stamp ensures that the distance between the cover glass and the glass slide is within the work distance of a 100× objective (0.2 mm).

**Cell Preparation.** Δ*fliC* and Δ*filC*Δ*pilA* isogenic mutants of *P. aeruginosa* strain ATCC 15692[35] were used in this study, which have the stable mutations of the genome. Strains were resuscitated on LB agar plates for 24 h at 37 °C. A monoclonal colony was inoculated in 1 mL of FAB minimal medium with 30 mM glutamate as the carbon source[36] and then grown in a shaker at 37 °C for 12 h. The bacterial cultures were diluted (1:100) in fresh FAB medium and cultured to an $OD_{600}$ of 0.8. The resultant culture was further diluted (1:50) and injected into the microfluidic device.

**Imaging of TIRDFM.** For the image formation, bacterial cells were illuminated by an evanescent wave from incident direction $\mathbf{k}_T$ at position $\mathbf{r}$ that refers to the lateral position in the $x-y$ plane, and the electric field image can be written as

$$\mathbf{E}_T(\boldsymbol{r}, d) = E_0 \exp(-\beta^{-1}d) \exp(i\mathbf{k}_T\cdot\mathbf{r}) \quad (1)$$

where $d$ refers to the distance of axial direction, $\beta$ is a decay constant of the evanescent wave, given by $\beta = \lambda/(4\pi\sqrt{(n_i \sin\theta)^2 - n_t^2})$, where $\lambda$ is the incident wavelength, $n_i$ is the refractive index of glass, $\theta$ is the incident angle, and $n_t$ is the refractive index of solution. The refraction index distribution of the cells $f(\mathbf{r},d)$ is illuminated with an evanescent wave incident from direction $\mathbf{k}_T$, with electric field $\mathbf{E}_T(\mathbf{r},d)$. Hence, the intensity of the TIRDFM image $I(\mathbf{r},d)$ is acquired by the convolution (*) of the electric field and the coherent point spread function $PSF_{coh}$,

$$I(\mathbf{r}, d) = |(f(\mathbf{r}, d)\mathbf{E}_T(\mathbf{r}, d))*PSF_{coh}|^2 \quad (2)$$

The coherent optical transfer function is partial of the spherical cap (Ewald). Irrespective of interference, intensity of the TIRDFM image has an exponential relationship to $d$, after the image is deconvolved by $PSF_{coh}$.

$$I(\mathbf{r}, d) \propto \exp(-\beta^{-1}d) \quad (3)$$

In our study, the evanescent wave was generated at the glass−liquid interface (interface between the glass slide and the liquid culture medium), and the bacterial cells attached on the glass slide will scatter light. The camera for imaging collected the scattered light, and the scattering intensity of each pixel was analyzed to calculate the separation distance between the body of the bacterial cell and the surface using eq 3. The image of distance information was created by displaying the calculated distance of each pixel as an image, where each element specifies the color for one pixel of the image, and the location of each pixel is the same with the scattered image.

**Data Processing.** Bright-field (BF) images and TIRDFM images of bacterial cells were acquired for every minute if not specified. The BF images were first subjected to the recognition of single cells via a MATLAB image-processing procedure.[26,37] The moving velocity of single bacterial cells was further analyzed using a sophisticated tracking algorithm.[26] The masks obtained from the BF image were shifted for 4 pixels along the incident direction $\mathbf{k}_T$ to merge the corresponding TIRDFM image. Assumed that the strongest scattering intensity of the bacterial cell is the nearest point to the surface, the relative distance of the bacterial cell can be calculated using eq 4

$$d = \log\frac{\max(I_b - I_d)}{I_b - I_d} \times \beta \quad (4)$$

where $I_b$ is the intensity of one pixel in the TIRDFM image, and $I_d$ is the corresponding intensity of the pixel in the dark image obtained in the absence of laser excitations. $I_b - I_d$ indicates the background correction of the TIRDFM image. max returns the maximum intensity of $I_b - I_d$ over all pixels of the cell regions in the corrected TIRDFM, and the location of the pixel with maximum intensity is recorded as the relative zero-distance position of the cell. In the time-course experiments, such as the process of cell growth or twitching on the surface, the relative zero-distance position corresponds to the maximum scattering intensity of the cell regions in all time-lapse images during the measurement period. We can use eq 4 to deduce changes in separation distance from changes in scattering intensity but cannot compute the absolute values of separation distance. Notably, in eqs 1 and 3, the scattering intensity also depends on the incident direction $\mathbf{k}_T$; we simplify this by only counting the bacterial cell whose long axis has an angle of 90 ± 5° with the incident direction $\mathbf{k}_T$.

## RESULT AND DISCUSSION

**Imaging of the Distance between Standard Spheres and the Surface.** We first verified the imaging effect of our p-TIRDFM microscopy using standard monodisperse PS particles (purchased from Thermo Fisher Scientific). As the PS particles are size-standard and highly uniform spheres, we aimed to image the scattered light of the particles absorbed on the surface to check the practicability of our p-TIRDFM method. PS particles (the diameter is 1 μm) suspended in FAB medium were injected into our designed microfluidic device to enable the attachment on the glass slide surface. A uniform PS sphere was thought to be attached on the surface with one nearest touchpoint, and the scattered light image should be concentric circles with a maximum diameter approximately of 1 μm. Figure 2A,B showed the scattered light image and the converted distance image of one attached PS particle, respectively. The brightest point in Figure 2A corresponds to the relative distance of 0 nm in Figure 2B, which is the nearest distance between the particle and the surface. Surrounding this point, both the distributions of scattering intensity and distance represent a set of concentric circles, which is in consistent with the uniform size of the standard particles. Figure 2B also showed that the mean distance extending from the center point to the edges is about 500 nm, which agrees well with the radius of the particles.

We further examined the separation distance between the different positions on the PS sphere and the surface. The black curve in Figure 2C represents the theoretic separating distance of different positions on a 1 μm sphere from the surface, which has the shape of a quarter of a circle. Square markers in Figure 2C are experimental data measured by calculating the mean values of pixels on the circumference of different concentric circles in Figure 2B. The results showed that the measured distance is fit to the theoretic data with good fidelity. We also monitored the change of relative distance between the attachment PS particles and the surface by calculating the mean scattering intensity at different time points and found that the distance showed a long-term stability over 10 min,



DOI: 10.1021/acs.langmuir.9b01378
Langmuir 2019, 35, 8860−8866

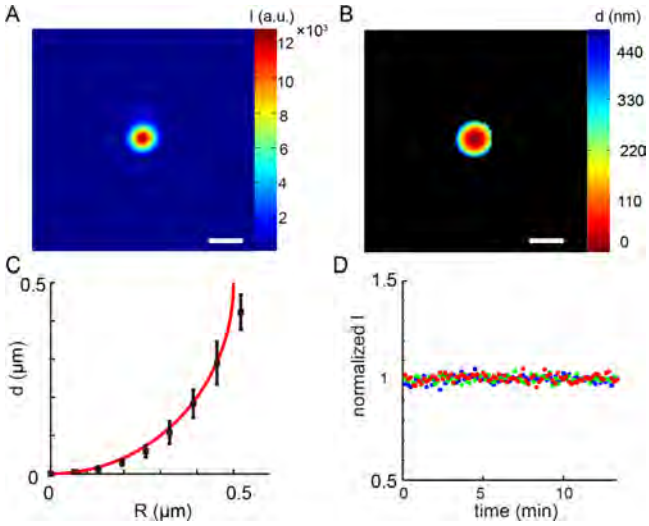


**Figure 2.** p-TIRDFM image of standard PS particles (1 $\mu$m). (A) Intensity distribution of a PS particle obtained by p-TIRDM. (B) Relative distance distribution of the PS particle converted by the p-TIRDM image is shown in Figure 2A. (C) Separation distance between the different positions on the PS sphere and the surface. The red curve represents the theoretic separation distance of different positions on a 1 $\mu$m sphere apart from the surface, which has the shape of a quarter of a circle. Square markers are experimental data measured from the distance distribution image by calculating the mean values of pixels on the circumference of different concentric circles. Error bars represent mean standard deviation from three attached particles. (D) Scattering intensity of PS particles attached on the glass surface showed a long-term stability. Markers with different colors represent different particles. The scale bar for all images is 2 $\mu$m.

which indicated that the PS particles attached on the surface uniformly and tightly (Figure 2D). Taken together, the results validated the functionality and feasibility of imaging distance using our TIRDFM method.

**Imaging of the Separation Distance between Attached Bacterial Cells and Surface.** Next, we aimed at investigating the distance between bacterial cells and the surface. For *P. aeruginosa*, two modes of motilities are driven by two types of appendages: a single polar flagellum and multiple TFP.[38] Swarming occurs by flagella to spread over a semisolid surface,[39] and twitching, a well-known surface motility mode, is mediated by TFP.[24] We monitored the change of scattered light of immobile cells when they are growing on the surface. The immobile cells that cannot move on the surface are Δ*filC*Δ*pilA* isogenic mutants of the wild type strain, where FilC is a key component of flagella, and PilA is the major component of TFP in *P. aeruginosa*. We injected Δ*filC*Δ*pilA* cells into the microfluidic device, and surface-attached cells were cultured under a shear strength (1.7 Pa). The shear stress enabled the long axis orientation of attached cells parallel to the flow and further ensured that the angle between the incident direction $\mathbf{k}_T$ and the long axis of the bacterial cell is same for all attached cells. The scattering intensity of the attached cells was imaged by TIRDFM, and the converted relative distance image of attached Δ*filC*Δ*pilA* cells was shown in Figure 3A (left panel). The distance image demonstrated that the middle of cell's body is the nearest position to the surface, and the two poles have a relative distance of 200 nm apart from the surface. Most interestingly, we observed that the relative distance varied with the cell growth on the surface (Figure 3A, right panel). The relative nearest touchpoint gradually shifted from the middle to the two poles and finally changed two touchpoints, respectively, for the two offspring with the development of the mother cell division (Figure 3B).

**Relationship between Twitching Velocity and Separation Distance When Bacteria Cells Move on the Surface.** To isolate twitching motility in *P. aeruginosa*, we then employed Δ*fliC* cells, the flagellum-deficient mutant of the wild type and monitored the twitching of Δ*fliC* cells on the glass slide surface of our designed microfluidic device using BF microscopy (1 fps). We simultaneously monitored the scattering intensity of the twitching cells using TIRDFM microscopy. The twitching velocity of the single bacterial cell was acquired by tracking each cell of BF images using automated tracking algorithms,[26] and the separation distance between the twitching cells and the surface was calculated by analyzing the corresponding TIRDFM image. Figure 4A,B showed two representative types of twitching motility: (A) mobile cell, whose average moving velocity is about 0.02 $\mu$m/s; (B) immobile cell, whose average moving velocity is about 0.0015 $\mu$m/s. Note that the velocity of the immobile cell was mainly attributed to the displacement of the centroid of the cell caused by growth.[26] The yellow lines in bright-field images indicated the movement trajectories of cells. The results showed that the separation distance from the surface fluctuates widely for the fast-twitching cell (mean distance during 30

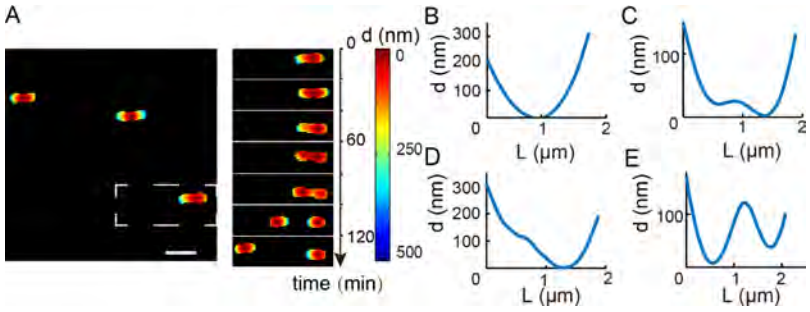


**Figure 3.** Relative separation distance of single cells on the surface. (A). Left panel: Relative separation distance image of Δ*filC*Δ*pilA* cells oriented perpendicular to the evanescent wave. Right panel: Relative separation distance image with the cell division. Interval of each image is 20 min. The scale bar is 2 $\mu$m, and color bar is the relative bacterial relative separation distance. (B–E) Relative separation distance along the long axis of the cell shown in A (right panel) at 20, 40, 60, and 80 min, respectively. (B) Middle of the bacterial body attached to the surface. (C,D) One pole of the bacterial body attached to the surface. (E) Bacterial Z-ring appears before cell division.



DOI: 10.1021/acs.langmuir.9b01378
*Langmuir* 2019, 35, 8860–8866

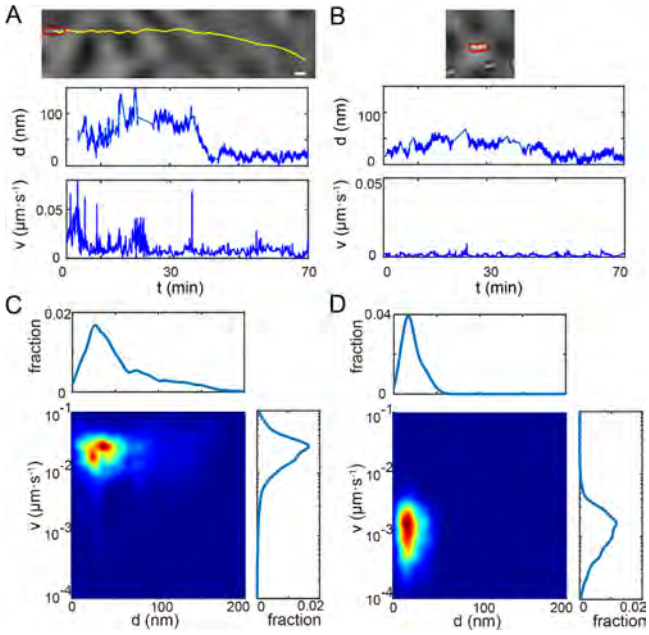


**Figure 4.** Relationship between the twitching velocity of Δ*filC* cells and the separation distance. (A,B) Representative separation distance apart from the surface of (A) a moving cell and (B) an immobile cell. Subpanels show the bright-field micrographs, the relative separation distance changes with time, and the instantaneous velocity with time, respectively. The scale bar for all micrographs is 2 $\mu$m. (C,D) Relative separation distance and velocity distribution of (C) moving cells whose average velocity was higher than 0.02 $\mu$m/s and (D) immobile cells whose average velocity was less than 0.002 $\mu$m/s. It has shown that the separation distance for the moving group has a larger fluctuation range than that for the immobile group. Upside: Distribution of relative distance; right side: distribution of velocity.

min: 68 nm; the maximum distance: 150 nm), while the distance is smaller and shows a relative stability for the nearly immobile cell (mean distance during 30 min: 22 nm; the maximum distance: 61 nm).

We further investigated the relationship between the twitching velocity and the separation distance statistically. We examined two distinctive groups of cells, which were classified artificially by their moving velocity. The cells with an average moving velocity less than 0.002 $\mu$m/s were defined as the immobile group, and the cells with an average moving velocity higher than 0.02 $\mu$m/s were identified as the moving group. Figure 4C,D displayed the map for illustration of the relationship between the twitching velocity and separation distance for the two groups, respectively, and the corresponding distributions of velocity and distance. It showed that the separation distance for the moving group has a lager fluctuation ranging from 0 to 100 nm than the immobile group (ranges: 0−50 nm), and the statistical data are in accordance with the above single cell results (Figure 4A,B). We then computed the coefficient of variation (CV; standard deviation divided by the mean) of separation distance to quantify the fluctuation. The moving group has a nearly 2-fold-higher of CV than the immobile group (moving group: a mean of 57 nm, standard deviation of 52 nm, and CV of 0.94; immobile group: a mean of 20 nm, standard deviation of 11 nm, and CV of 0.55). The results further confirmed the large fluctuation of separation distance for the fast-moving cells.

In this study, we presented an imaging method combining TIRDFM with microfluidic technology, and we obtained high-resolution images of scattered light when bacterial cells attached on the glass-slide surface. Based on the nature of the evanescent wave, we deduced the relative separation distance by analyzing the measured scattering intensity, and furthermore, we observed the changes of distances between the bacterial cells and the surface sensitively on the nanometer scale. Compared with the other nanoscale imaging methods, such as the atomic force microscope[31,32,40] and electron microscope,[29] our established TIRDFM method does not need surface modification, freezing, or vacuum, and most importantly, we can image the individual bacterial cells with high image acquisition frequency in real time for a long time. Besides, the high-resolution light-based microscopy techniques, such as image-scanning microscopy,[41] stimulated emission depletion microscopy,[42] photoactivated localization microscopy,[43] and stochastic optical reconstruction microscopy,[44] can image the cell morphology and structures at the length scale of a sub-100 nm, but the *z*-axis resolution is still insufficient for investigating the change of separation distance apart from the surface.

In bacteriology, biofilm initialization, development, and formation depend critically on how planktonic bacterial cells adjust their motility mechanisms to acclimate to the surface circumstances.[45] Our results established the relationship between the twitching velocity and the separation distance when bacterial cells move on a surface, and this connection may help us to understand the surface-related behaviors during the biofilm formation. The relative further separation distance of the fast-moving bacterial cells could enable them to detach from the surface to colonize new places more easily, which may be a possibility of the detaching mechanism in early bacterial biofilm communities.[46] We expect our TIRDFM method of imaging bacterial separation distance to be widely applicable. The TIRDFM method is well compatible with other microscopies, such as wide-field and fluorescence microscopies. Combining with other microscopies, one now should be able to monitor the cell behaviors on the surface, including twitching motility, metabolism and conjugation, and the separation distance simultaneously. The study of cell basic physiological processes in the formation of bacterial biofilms on a surface, especially at the early stage, shows an important field of fundamental research, and our method has the potential to accelerate this process. In addition, it should also be possible to study the interaction of living bacterial cells with different surfaces using the TIRDFM method.

## CONCLUSIONS

In summary, we have shown that the scattered images induced by the evanescent wave enabled the observation of separation distance between the attached bacterial cells and the surface. We first observed that a standard PS sphere attached on the glass slide with one nearest touchpoint and the separation distance has virtually no change during a long period. For bacterial cells, the bulk cells attached to the surface with one nearest touchpoint at first, but when they are growing on the surface, the relative nearest touchpoint gradually shifted from the middle to the two poles and finally changed two touchpoints, respectively, for the two offspring. We further established the relationship between the twitching velocity and the separation distance when cells move on the surface, and the results indicated that the moving cells are a considerable distance apart from the surface, and the separation distance fluctuated widely due to twitching.



DOI: 10.1021/acs.langmuir.9b01378
*Langmuir* 2019, 35, 8860−8866

Moreover, the approach provides a promising methodology for leveraging the tools of evanescent wave-based microscopy to explore the interaction between bacterial cells and surfaces, and the surface-related basic research in the process of biofilm development. We anticipate that the TIRFDM method, combining with other methods, including fluorescent labels, single-molecule localization, and fluorescence microscopy, will make it a commonly used tool in bacteriology, even in life sciences.

## AUTHOR INFORMATION


### Corresponding Authors

*E-mail: xingxc@ustc.edu.cn. Phone: +86-551-63606925. Fax: +86-551-63606743 (X.X.).

*E-mail: fjinustc@ustc.edu.cn (F.J.).

### ORCID

Shuai Yang: 0000-0001-8325-4994

Fan Jin: 0000-0003-2313-0388

### Present Address

⊥Fan Jin, Institute of Synthetic Biology, Shenzhen Institutes of Advanced Technology, Chinese Academy of Sciences, Shenzhen 518055, China.


### Author Contributions

A.X. and S.Y. contributed equally to this work. F.J. and X.X. conceived the project. A.X., S.Y., R.Z., and L.N. performed the experiments. A.X. and S.Y. contributed jointly to data interpretation and manuscript preparation. All authors have given approval to the final version of the manuscript.

### Notes

The authors declare no competing financial interest.

## ACKNOWLEDGMENTS

The National Natural Science Foundation of China (31700745, 21774117, and 31700087) and the Fundamental Research Funds for the Central Universities (WK2340000066, WK2030020023, and WK3450000003) supported this work.

## REFERENCES


(1) Wilks, P. A., Jr.; Hirschfeld, T. *Internal Reflection Spectroscopy*; John Wiley and Sons: New York 1967.

(2) Prieve, D. C.; Luo, F.; Lanni, F. Brownian motion of a hydrosol particle in a colloidal force field. *Faraday Discuss. Chem. Soc.* **1987**, *83*, 297−307.

(3) Prieve, D. C.; Frej, N. A. Total internal reflection microscopy: a quantitative tool for the measurement of colloidal forces. *Langmuir* **1990**, *6*, 396−403.

(4) Walz, J. Y. Measuring particle interactions with total internal reflection microscopy. *Curr. Opin. Colloid Interface Sci.* **1997**, *2*, 600−606.

(5) Axelrod, D.; Thompson, N. L.; Burghardt, T. P. Total internal reflection fluorescent microscopy. *J. Microsc.* **1983**, *129*, 19−28.

(6) Axelrod, D. Total Internal Reflection Fluorescence Microscopy in Cell Biology. *Traffic* **2001**, *2*, 764−774.

(7) Fort, E.; Grésillon, S. Surface enhanced fluorescence. *J. Phys. D: Appl. Phys.* **2008**, *41*, 013001.

(8) Ueno, H.; Nishikawa, S.; Iino, R.; Tabata, K. V.; Sakakihara, S.; Yanagida, T.; Noji, H. Simple Dark-Field Microscopy with Nanometer Spatial Precision and Microsecond Temporal Resolution. *Biophys. J.* **2010**, *98*, 2014−2023.

(9) von Olshausen, P.; Rohrbach, A. Coherent total internal reflection dark-field microscopy: label-free imaging beyond the diffraction limit. *Opt. Lett.* **2013**, *38*, 4066−4069.

(10) Hill, D. J.; Pinion, C. W.; Christesen, J. D.; Cahoon, J. F. Waveguide Scattering Microscopy for Dark-Field Imaging and Spectroscopy of Photonic Nanostructures. *ACS Photonics* **2014**, *1*, 725−731.

(11) Jünger, F.; Olshausen, P. v.; Rohrbach, A. Fast, label-free super-resolution live-cell imaging using rotating coherent scattering (ROCS) microscopy. *Sci. Rep.* **2016**, *6*, 30393.

(12) Jain, P. K.; Lee, K. S.; El-Sayed, I. H.; El-Sayed, M. A. Calculated Absorption and Scattering Properties of Gold Nanoparticles of Different Size, Shape, and Composition: Applications in Biological Imaging and Biomedicine. *J. Phys. Chem. B* **2006**, *110*, 7238−7248.

(13) Hu, M.; Novo, C.; Funston, A.; Wang, H.; Staleva, H.; Zou, S.; Mulvaney, P.; Xia, Y.; Hartland, G. V. Dark-field microscopy studies of single metal nanoparticles: understanding the factors that influence the linewidth of the localized surface plasmon resonance. *J. Mater. Chem.* **2008**, *18*, 1949−1960.

(14) Kelly, K. L.; Coronado, E.; Zhao, L. L.; Schatz, G. C. The Optical Properties of Metal Nanoparticles: The Influence of Size, Shape, and Dielectric Environment. *J. Phys. Chem. B* **2003**, *107*, 668−677.

(15) Huang, X.; El-Sayed, I. H.; Qian, W.; El-Sayed, M. A. Cancer Cell Imaging and Photothermal Therapy in the Near-Infrared Region by Using Gold Nanorods. *J. Am. Chem. Soc.* **2006**, *128*, 2115−2120.

(16) Schultz, S.; Smith, D. R.; Mock, J. J.; Schultz, D. A. Single-target molecule detection with nonbleaching multicolor optical immunolabels. *Proc. Natl. Acad. Sci. U.S.A.* **2000**, *97*, 996.

(17) Murphy, C. J.; Gole, A. M.; Stone, J. W.; Sisco, P. N.; Alkilany, A. M.; Goldsmith, E. C.; Baxter, S. C. Gold Nanoparticles in Biology: Beyond Toxicity to Cellular Imaging. *Acc. Chem. Res.* **2008**, *41*, 1721−1730.

(18) Schulz, O.; Pieper, C.; Clever, M.; Pfaff, J.; Ruhlandt, A.; Kehlenbach, R. H.; Wouters, F. S.; Grosshans, J.; Bunt, G.; Enderlein, J. Resolution doubling in fluorescence microscopy with confocal spinning-disk image scanning microscopy. *Proc. Natl. Acad. Sci. U.S.A.* **2013**, *110*, 21000.

(19) Kner, P.; Chhun, B. B.; Griffis, E. R.; Winoto, L.; Gustafsson, M. G. L. Super-resolution video microscopy of live cells by structured illumination. *Nat. Methods* **2009**, *6*, 339.

(20) Huang, B.; Bates, M.; Zhuang, X. Super-Resolution Fluorescence Microscopy. *Annu. Rev. Biochem.* **2009**, *78*, 993−1016.

(21) Schermelleh, L.; Heintzmann, R.; Leonhardt, H. A guide to super-resolution fluorescence microscopy. *J. Cell Biol.* **2010**, *190*, 165.

(22) Lang, T.; Wacker, I.; Wunderlich, I.; Rohrbach, A.; Giese, G.; Soldati, T.; Almers, W. Role of Actin Cortex in the Subplasmalemmal Transport of Secretory Granules in PC-12 Cells. *Biophys. J.* **2000**, *78*, 2863−2877.

(23) Skerker, J. M.; Berg, H. C. Direct observation of extension and retraction of type IV pili. *Proc. Natl. Acad. Sci. U.S.A.* **2001**, *98*, 6901.

(24) Mattick, J. S. Type IV Pili and Twitching Motility. *Annu. Rev. Microbiol.* **2002**, *56*, 289−314.

(25) Harshey, R. M. Bacterial Motility on a Surface: Many Ways to a Common Goal. *Annu. Rev. Microbiol.* **2003**, *57*, 249−273.

(26) Ni, L.; Yang, S.; Zhang, R.; Jin, Z.; Chen, H.; Conrad, J. C.; Jin, F. Bacteria differently deploy type-IV pili on surfaces to adapt to nutrient availability. *npj Biofilms Microbiomes* **2016**, *2*, 15029.

(27) Jin, F.; Conrad, J. C.; Gibiansky, M. L.; Wong, G. C. L. Bacteria use type-IV pili to slingshot on surfaces. *Proc. Natl. Acad. Sci. U.S.A.* **2011**, *108*, 12617.

(28) Dufrêne, Y. F. Towards nanomicrobiology using atomic force microscopy. *Nat. Rev. Microbiol.* **2008**, *6*, 674.

(29) Prigent-Combaret, C.; Prensier, G.; Le Thi, T. T.; Vidal, O.; Lejeune, P.; Dorel, C. Developmental pathway for biofilm formation in curli-producing Escherichia coli strains: role of flagella, curli and colanic acid. *Environ. Microbiol.* **2000**, *2*, 450−464.

(30) Gould, S. A. C.; Drake, B.; Prater, C. B.; Weisenhorn, A. L.; Manne, S.; Hansma, H. G.; Hansma, P. K.; Massie, J.; Longmire, M.; Elings, V.; Northern, B. D.; Mukergee, B.; Peterson, C. M.; Stoeckenius, W.; Albrecht, T. R.; Quate, C. F. From atoms to integrated circuit chips, blood cells, and bacteria with the atomic force microscope. *J. Vac. Sci. Technol., A* **1990**, *8*, 369−373.




DOI: 10.1021/acs.langmuir.9b01378
*Langmuir* 2019, 35, 8860−8866

(31) Van Der Hofstadt, M.; Hüttener, M.; Juárez, A.; Gomila, G. Nanoscale imaging of the growth and division of bacterial cells on planar substrates with the atomic force microscope. *Ultramicroscopy* **2015**, *154*, 29−36.
(32) Ando, T. High-speed atomic force microscopy coming of age. *Nanotechnology* **2012**, *23*, 062001.
(33) Ando, T. High-speed atomic force microscopy and its future prospects. *Biophys. Rev.* **2018**, *10*, 285−292.
(34) Qin, D.; Xia, Y.; Whitesides, G. M. Soft lithography for micro- and nanoscale patterning. *Nat. Protoc.* **2010**, *5*, 491.
(35) Shrout, J. D.; Chopp, D. L.; Just, C. L.; Hentzer, M.; Givskov, M.; Parsek, M. R. The impact of quorum sensing and swarming motility on Pseudomonas aeruginosa biofilm formation is nutritionally conditional. *Mol. Microbiol.* **2006**, *62*, 1264−1277.
(36) Heydorn, A.; Givskov, M.; Ersbøll, B. K.; Parsek, M. R.; Hentzer, M.; Molin, S. Experimental reproducibility in flow-chamber biofilms. *Microbiology* **2000**, *146*, 2409−2415.
(37) Yang, S.; Cheng, X.; Jin, Z.; Xia, A.; Ni, L.; Zhang, R.; Jin, F. Differential Production of Psl in Planktonic Cells Leads to Two Distinctive Attachment Phenotypes in Pseudomonas aeruginosa. *Appl. Environ. Microbiol.* **2018**, *84*, e00700−18.
(38) Conrad, J. C.; Gibiansky, M. L.; Jin, F.; Gordon, V. D.; Motto, D. A.; Mathewson, M. A.; Stopka, W. G.; Zelasko, D. C.; Shrout, J. D.; Wong, G. C. L. Flagella and Pili-Mediated Near-Surface Single-Cell Motility Mechanisms in P. aeruginosa. *Biophys. J.* **2011**, *100*, 1608−1616.
(39) Kohler, T.; Curty, L. K.; Barja, F.; van Delden, C.; Pechere, J.-C. Swarming of Pseudomonas aeruginosa Is Dependent on Cell-to-Cell Signaling and Requires Flagella and Pili. *J. Bacteriol.* **2000**, *182*, 5990.
(40) Zorila, F. L.; Ionescu, C.; Craciun, L. S.; Zorila, B. Atomic force microscopy study of morphological modifications induced by different decontamination treatments on Escherichia coli. *Ultramicroscopy* **2017**, *182*, 226−232.
(41) Müller, C. B.; Enderlein, J. Image Scanning Microscopy. *Phys. Rev. Lett.* **2010**, *104*, 198101.
(42) Hell, S. W.; Wichmann, J. Breaking the diffraction resolution limit by stimulated emission: stimulated-emission-depletion fluorescence microscopy. *Opt. Lett.* **1994**, *19*, 780−782.
(43) Betzig, E.; Patterson, G. H.; Sougrat, R.; Lindwasser, O. W.; Olenych, S.; Bonifacino, J. S.; Davidson, M. W.; Lippincott-Schwartz, J.; Hess, H. F. Imaging Intracellular Fluorescent Proteins at Nanometer Resolution. *Science* **2006**, *313*, 1642.
(44) Rust, M. J.; Bates, M.; Zhuang, X. Sub-diffraction-limit imaging by stochastic optical reconstruction microscopy (STORM). *Nat. Methods* **2006**, *3*, 793.
(45) O'Toole, G. A.; Kolter, R. Flagellar and twitching motility are necessary forPseudomonas aeruginosabiofilm development. *Mol. Microbiol.* **1998**, *30*, 295−304.
(46) Lee, C. K.; de Anda, J.; Baker, A. E.; Bennett, R. R.; Luo, Y.; Lee, E. Y.; Keefe, J. A.; Helali, J. S.; Ma, J.; Zhao, K.; Golestanian, R.; O'Toole, G. A.; Wong, G. C. L. Multigenerational memory and adaptive adhesion in early bacterial biofilm communities. *Proc. Natl. Acad. Sci. U.S.A.* **2018**, *115*, 4471.



DOI: 10.1021/acs.langmuir.9b01378
*Langmuir* 2019, 35, 8860−8866